# Investigation of reaction mechanisms in the chemical vapor deposition of al from DMEAA

George M Psarellis, Ioannis G Aviziotis, Thomas Duguet, Constantin Vahlas, Eleni D Koronaki, Andreas Boudouvis

# Investigation of reaction mechanisms in the chemical vapor deposition of al from DMEAA

George M. Psarellis [a], Ioannis G. Aviziotis [a,b,⇑], Thomas Duguet [b], Constantin Vahlas [b], Eleni D. Koronaki [a], Andreas G. Boudouvis [a]

[a] School of Chemical Engineering, National Technical University of Athens, Heroon Polytechniou 9, 15780 Zografou, Greece

[b] CIRIMAT, CNRS, Université de Toulouse, 4 alleé Emile Monso, BP 44362, 31030 Toulouse cedex 4, France

## highlights

- Experimental and computational analysis of Al CVD from DMEAA.
- Detailed chemistry mechanism with side reactions.
- $AlH_3$ gas phase oligomerization and surface dehydrogenation steps.
- Prediction of experimentally measured deposition rate.
- Decrease of deposition rate due to $AlH_3$ oligomerization and surface desorption.

## article info

Article history:
Received 17 July 2017
Received in revised form 16 November 2017
Accepted 4 December 2017 Available online 6 December 2017

Keywords:
Modeling aluminum CVD
Reaction mechanisms
Alane oligomerization
Alane dehydrogenation
Surface desorption
Surface site reactions

## abstract

We propose a novel reaction scheme for the chemical vapor deposition (CVD) of Al films on substrates from dimethylethylamine alane (DMEAA), supported by the prediction of the Al deposition rate as a func-tion of process temperature. The scheme is based on gas phase oligomerizations of alane which form a substantial amount of intermediates. Combined with reversible surface dehydrogenation steps, the global deposition reaction is composed of a set of 12 chemical reactions. This new scheme entails four interme-diates and includes side reactions that play an important role in the formation of Al thin films. The chem-istry mechanism is incorporated in a 2D Computational Fluid Dynamics (CFD) model of the CVD reactor setup used for the experimental investigation. The simulation predictions of the Al deposition rate are in good agreement with corresponding experimental measurements. The success of this novel reaction pathway lies in its ability to capture the abrupt decrease of the deposition rate at temperatures above 200 LC, which is attributed to the gas phase consumption of alane along with its increased desorption rate from the film surface.



## 1. Introduction

Thin aluminum (Al) solid films show advantageous properties, such as high electrical conductivity (Lee et al., 2014) and significant resistance to electromigration (Tan and Roy, 2007) and corrosion (Hamasha et al., 2011) rendering them ideal constituents for inte-grated circuits. Moreover, Al can be applied as component in metallic alloys, such as $AlFe_3$ (Sundman et al., 2009), $AlPt_3$ (Delmas et al., 2005) or $Al_{13}Fe_4$ (Armbrüster et al., 2012) to provide advanced materials with enhanced mechanical and thermal prop erties, catalytic activity and wetting properties, respectively. Chemical vapor deposition (CVD) of Al has been applied for the industrial production of wires, multilevel interconnections of ultra large scale integrated circuits (ULSI) (Yun et al., 1998a; Masu et al., 1994), micro-plugs and electric interconnects (Amazawa et al., 1998) and for the processing of films composed of the approximant c-$Al_4Cu_9$ (Aloui et al., 2012).

Compared to other deposition techniques, such as PVD, mag-netron sputtering or ALD, CVD combines high throughput, versatil-ity, successful control of the film microstructural characteristics and most importantly the conformal coverage of non-line-of-sight surfaces (Kleijn et al., 2007; Vahlas, 2010).

In order to control the process and achieve the maximum potential, the chemical mechanisms as well as the transport phe-nomena occurring in the CVD reactor have to be investigated and understood (Aviziotis, 2016). In particular, it is suggested that detailed reaction pathways have to be considered instead of reduced schemes, since various intermediates can play a signifi-cant role in the overall deposition process (Aviziotis et al., 2017; Kuwana et al., 2006; Kleijn, 2000). Despite such well admitted requirements, limited research is available on the detailed chem-istry scheme of Al-CVD using a DMEAA (dimethylethylamine alane) precursor; i.e., a commonly used precursor, allowing pro-cessing of pure Al films at low temperature (Simmonds et al., 1994; Luo and Gladfelter, 2009).

Several studies have been reported dealing with the deposition behavior and chemistry mechanisms of DMEAA on the surface. Han et al. (1994) proposed that the rate limiting step is either the decomposition of DMEAA on the surface of the substrate or the desorption of the molecular hydrogen from the surface, or a com-bination of these two reaction steps. Furthermore, Kim et al. (1996), suggested that DMEAA may dissociate in the gas phase, at temperature values higher than 170 LC leading to the formation of powders.

⇑ Corresponding author at: School of Chemical Engineering, National Technical University of Athens, Heroon Polytechniou 9, 15780 Zografou, Greece.
E-mail address: javiziot@chemeng.ntua.gr (I.G. Aviziotis).

DMEAA may also decompose in the gas phase. Yun et al. (1998b) reported the value of the activation energy of this gas phase decomposition by performing FTIR analysis of the gas phase. They also confirmed the formation of powder at elevated temper-ature as a result of oligomerization reactions that $AlH_3$ may undergo in the gas phase. Finally, the experimental data reported in the literature (Aviziotis et al., 2015; Jang et al., 1998; Kim et al., 1996; Yun et al., 1998a, 1998b) show that the Al deposition rate decreases considerably above 200 LC. Hypotheses have been formulated to explain this behavior including the increased gas phase dissociation rate of DMEAA as a competitive mechanism to the deposition process (Kim et al., 1996), the increased desorption rate of the precursor (Choy, 2003) or the recombinative desorption of $H_2$ from the monohydride adsorbate $H_{ads}$ which occurs at high temperature on Si(1 0 0) (Robinson and Rogers, 2000).

Nakajima et al. (2003) performed quantum chemical calcula-tions to determine the mechanisms occurring on the surface dur-ing the process. They suggested that the precursor is adsorbed on the surface where it dissociates to $AlH_3$ and DMEA. DMEA is rapidly desorbed from the surface whereas $AlH_3$ undergoes several dehy-drogenation steps before the deposition of atomic Al. The above-mentioned report does not consider reactions in the gas phase although they can have a significant effect on the Al deposition rate.

In previous works (Xenidou et al., 2007, 2010), it was suggested that one gas phase and one surface reaction can capture the depo-sition of Al films. These reactions involve the gas phase and the surface dissociation of DMEAA, as follows:

$$DMEAA_{(g)} \rightarrow DMEA_{(g)} + AlH_{3(g)} \quad (1)$$

$$DMEAA_{(g)} \rightarrow Al_{(s)} + DMEA_{(g)} + 3/2H_{2(g)} \quad (2)$$

Although deposition profiles on substrates correlate satisfacto-rily with the experimental data, the behavior of the deposition rate as a function of the substrate's temperature is investigated at only four different temperature values. Hence, there is limited data to extract useful information concerning the reaction mechanisms of the process. Recently, we have reported a combined experimen-tal and computational study (Aviziotis et al., 2015) for the investi-gation of the average deposition rate as a function of the surface temperature, in a more detailed temperature range. By incorporat-ing the reaction scheme of Eqs. (1) and (2) into the computational model, we managed to predict satisfactorily the deposition rate at the low temperature regime but not at higher temperature. We have deduced that the chemistry scheme that consists of the above-mentioned reactions along with first-order Arrhenius type kinetics do not predict with sufficient accuracy the experimental data, especially at temperatures higher than 200 LC. Thus, a more detailed chemistry pathway is required with the corresponding kinetic mechanisms for the description of the phenomena occur-ring at higher temperatures.

The present work provides a combined experimental and theo-retical investigation of the deposition of Al from DMEAA. A two-dimensional (2D) macroscopic model is developed based on first principles, i.e., the conservation of mass, momentum and energy, and it accounts for transport mechanisms in the bulk of the CVD reactor. In addition, the macroscopic model includes for the first time a detailed chemistry model based on comprehensive litera-ture information and describes the gas phase and the surface reac-tions of the precursor and pertinent. The predictive capability of the model is validated through the comparison of the theoretical output with corresponding experimental measurements, namely with the deposition rate determined as a function of the deposition temperature.

## 2. Experimental

Deposition of Al films is performed in a vertical, cylindrical, stagnant flow, warm wall, stainless steel MOCVD reactor which has been described in detail in Xenidou et al. (2010). The prepara-tion of the silicon (Si) coupons used as substrates supported on a susceptor is described in our previous work (Aviziotis et al., 2015). DMEAA is synthesized by NanoMePS[1] and is supplied in a stainless steel bubbler equipped with a 3-valve bypass system. It is maintained at 3 LC permanently; i.e. below the freezing point of the compound, thus strongly limiting its degradation (Matsuhashi et al., 1999). It is thermally regulated to 7 LC during the experiments. At this temperature, the partial pressure of DMEAA is 0.7 Torr (Frigo et al., 1994). Pure nitrogen (99.998%, Air Products) is fed through computer-driven mass flow controllers (MKS).

Experiments are performed at fixed conditions, namely total pressure of the reactor $P_{tot}$ = 10 Torr, thermal regulation of the lines $T_{lines}$ = 100 LC and of the walls of the reactor $T_{walls}$ = 75 LC, while the $N_2$ dilution gas flow ($Q_{N2,dilution}$) and the $N_2$ carrier gas flow through the precursor ($Q_{N2,prec}$) equal 305 and 25 standard cubic centimeters per minute (sccm), respectively. Considering the relation proposed by Hersee and Ballingal (1990), these condi-tions yield a maximum flow rate $Q_{prec}$ of DMEAA in the input gas, equal to 2 sccm. However, as we have shown in Aviziotis et al. (2015), the effective mass inflow rate of the precursor equals 1.85 sccm. A perforated plate (shower plate), located above the susceptor, enhances the entering gas distribution and mixing.

Independent experiments are performed at eight different sub-strate temperature values, $T_s$, in the range 139–241 LC. $T_s$ was cal-ibrated under rough vacuum by attaching a thermocouple to the surface of a dummy Si coupon. The deposition time is 1 h in all experiments, including the time required for the nucleation to take place at each $T_s$, that is the incubation time. We have referred in detail to the importance of the incubation time for the determina-tion of net deposition rate in Aviziotis et al. (2015). The deposition rate is evaluated directly by weight difference (±10 lg) of the sub-strates before and after deposition, using a microbalance (Sartorius).

The microstructural characteristics of the films such as morpho-logical observations of the surface and the determination of the surface roughness both experimentally and computationally have been reported in our previous works (Aviziotis et al., 2015, 2016) and it is not a matter of investigation in the present work.

## ~~3. Process~~ modeling – Chemistry mechanism

For the investigation of the chemistry pathway and the kinetic mechanisms of Al films growth, a 2D model of the MOCVD reactor is built, based on the governing equations describing the transport phenomena and the chemical reactions inside the reactor. The reactor model is presented in Fig. 1 to assist the reader on the iden-tification of various part discussed in the next section. The continu-ity, momentum, energy and the species transport equations augmented with realistic boundary conditions (Cheimarios et al., 2010; Deen, 1998) are discretized with the finite volume method and the resulting system of equations is solved with Ansys/Fluent (Ansys/Fluent, 2009).

### 3.1. Gas phase reactions and kinetics

DMEAA can be easily decomposed in the gas phase, as it is indi-cated by its low decomposition energy compared to other gas phase reactions, as shown in Table 1 (Xenidou et al., 2010; Yun et al., 1998b). The products of this decomposition are DMEA and $AlH_3$. It is known and accounted for in this work that metal hydrides such as $AlH_3$ can form polymers at high temperature (Aitken and Harrod, 1985; Kawamura et al., 2003; Michos et al., 2016).

1 www.nanomeps.fr, last visited July 5, 2017.

Kawamura et al. (2003) investigated the gas phase polymer-ization of alane and studied the kinetics of the dimerization, trimerization and other related oligomer producing reactions (oli-gomers with 2–7 Al atoms) both linear and cyclic. They calculated the activation energies and the pre-exponential factors by employ-ing first-principles calculations with a plane-wave basis and a method of a linear combination of atomic-orbitals. Our model accounts only for the dimerization and trimerization reactions, since we aim at incorporating a mechanism of depletion of $AlH_3$ and not the polymerization process of this compound per se.

The gas phase reactions (G1–G3) with their corresponding ener-gies are summarized in Table 1. For this scheme, we modify the Arrhenius law implemented in Fluent (Ansys/Fluent 2009) to account for the stoichiometry of the reactions. The Arrhenius reac-tion rate corresponding to these reactions is:

$$R_{Gi} \text{ ¼ } k_{0;Gi} \exp \left( \frac{E_{a;G}}{RT_{gas}} \right)^{i} PC_i ; \quad \text{ð3Þ}$$

where $R_{Gi}$ denotes the reaction identity, $C^n_i$ the gas phase concentra-tion of the corresponding species, i and the order of the reaction, n, $E_{a;Gi}$ is the activation energy and $T_{gas}$ is the temperature of the gas phase in the reactor. The pre-exponential factor, $k_{0;Gi}$ , of the first reaction is provided by Yun et al. (1998b). The pre-exponential fac-tors of the two other reactions are fitted to the experimental data. In order to fit the unknown pre-exponential factors of the gas-phase reactions, the process is simulated first at the high-temperature regime, where the gas phase reaction rates are high and gas phase processes become dominant for the deposition process. The pre-exponential factors fitted in the diffusion-limited regime are applied for the simulation of the process in the whole temperature range for a fine tuning. Values of the pre-exponential factors for each reaction are summarized in Table 1.

As indicated in Table 1, the oligomerization reactions (G2–G3) have much higher activation energies than the decomposition of the precursor (G1). This would explain the activation of these reac-tions at high temperature with a subsequent consumption of $AlH_3$ prior reaching the deposition surface.

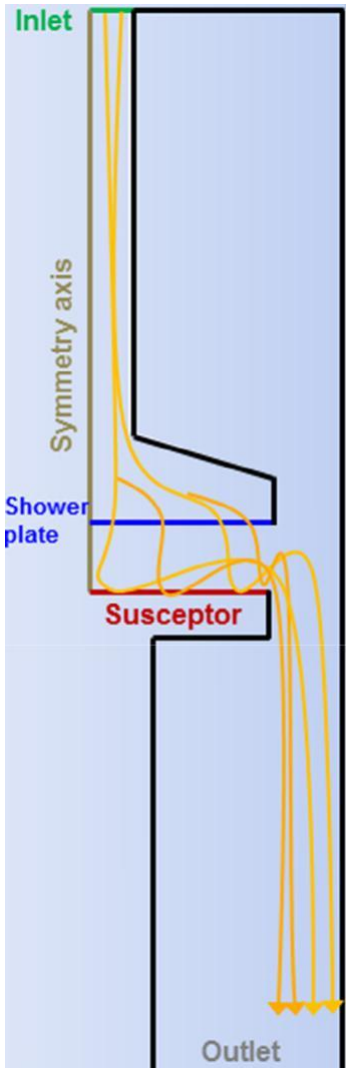


Fig. 1. The 2D geometry of the reactor built for the simulation of the CVD of Al.

### 3.2. Surface reactions

The surface reaction pathway that we propose is similar to the one reported by Nakajima et al. (2003). The $AlH_3$ which does not

Table 1
The gas phase reaction scheme of the CVD of Al from DMEAA. The Arrhenius rate expressions are given by Eq. (3).

| ID | Reaction | Pre-exponential factor | Activation energy (kJ mol $^{1}$) |
|---|---|---|---|
| G1 | DMEAA ? DMEA + $AlH_3$ | 2.0 $10^7$ s $^{1a}$ | 40.06[a] |
| G2 | 2$AlH_3$ ? $Al_2H_6$ | 2.55 $10^{20}$ m$^3$ kmol $^{1}$ s $^{1b}$ | 118.0[c] |
| G3 | $AlH_3$ + $Al_2H_6$ ? $Al_3H_9$ | 7.75 $10^{20}$ m$^3$ kmol $^{1}$ s $^{1b}$ | 90.70[c] |

a Yun et al. (1998b).
b This work.
c Kawamura et al. (2003).

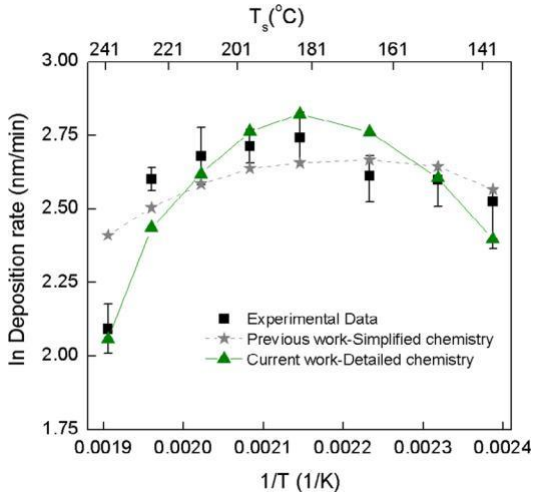


Fig. 2. The Arrhenius plot of the CVD of Al from DMEAA. Experimental measure-ments (squares) and computational predictions with the detailed (solid line with triangles) and the simplified (dashed line with stars) chemistry mechanisms are shown.

undergo gas phase oligomerization, reaches and is adsorbed on the heated surface. According to Nakajima et al. (2003), it occupies three surface sites during its adsorption, one for the Al atom itself and two for the H atoms. The third H atom is located above the Al atom in the opposite direction to the surface. This inverted tetrahe-dron structure of $AlH_3$ has been also reported by Chaudhuri et al. (2008). For the activation energy of the adsorption of $AlH_3$ on the surface we apply the value extracted from the experimental Arrhe-nius plot (see below Fig. 2) while for that of the $AlH_3$ desorption the value reported by Chaudhuri et al. (2008).

Once adsorbed on the surface, $AlH_3$ begins to undergo reversible dehydrogenation steps for the formation of $AlH_2$, AlH and eventu-ally Al. The surface structures of $AlH_2$ and AlH are similar to that of $AlH_3$, i.e., they occupy two and one surface sites, respectively. The surface reactions with their corresponding activation energies are summarized in Table 2, where S denotes the unoccupied surface sites.

The surface decomposition of $AlH_3$ (SR2), its reverse reaction (SR3), the surface recombination of AlH with H (SR5) and the recombinative desorption of H (SR8) are rather easy due to their small activation energies. In contrast, the reaction resulting in the deposition of Al (SR7) seems more difficult to proceed since its activation energy is quite high compared to the other reactions.

As we briefly mention above, the surface processes of $AlH_3$ and its surface decomposition products involve their surface structures and the occupation of surface sites. That is, inhibition of surface availability due to the adsorbed species may occur during the pro-cess. For this reason, we implement a modified Arrhenius type expression:

$$R_{Si} \frac{1}{4} k_{0;Si} \exp\left(\frac{RT_s^{j}}{E_{a;S}}\right) PC_i ; \quad \text{ð4Þ}$$

Here $R_{Si}$ denotes the reaction identity, $E_{a;Si}$ is the activation energy of each reaction and $T_s$ is the temperature of the substrate. The modification of this rate equation lies in the concentration term, $C_i$, which expresses the concentration of each adsorbed species as a function of the surface coverage and the site density:

$$C_i \frac{1}{4} h_i \quad d; \quad \text{ð5Þ}$$

where $h_i$ is the coverage of each adsorbed species and d is the site density in kmol $m^{2}$ as required by the computational software (Ansys/Fluent, 2009). For the site density we apply the value of $10^{9}$ kmol $m^{2}$, a value in the range of the one reported by Letterman and Iyer (1985).

The pre-exponential factors, $k_{0;Si}$ , are fitted to the experimental data. For the fitting of these parameters, the process is first simu-lated at the reaction-limited regime where surface reactions are more important than gas phase reactions or diffusion mechanisms. Then, simulations are performed in the whole temperature range for the better fitting of the pre-exponential factors. Exception to this process are reactions SR7 and SR9 which describe the desorp-tion of $H_{ads}$ and $AlH_{3,ads}$. Since desorption is favored at high tem-perature, the pre-exponential factors of these reactions are first fitted to the experimental data at the high temperature regime. It is noted here that Nakajima et al. (2003) determined the values of the pre-exponential factors of reactions SR2–SR5 and SR7–SR8 based on transition state theory calculations. Thus, these values correspond to vibrational frequencies (s-1) at the atomic scale. At the macroscopic level where we model the process, we apply apparent pre-exponential factors rather than vibrational frequen-cies. Thus, we fit these kinetic parameters instead of using the val-ues reported by Nakajima et al. (2003). Nevertheless, we maintain unchanged the ratio of the pre-exponential factor of the forward reactions to that of the reverse reactions, for consistency to their work.

## 4. Results and discussion

Fig. 2 presents the Arrhenius plot of the process where both experimental measurements (squares) and computational predic-tions are shown. Error bars attached to the experimental results correspond to the minimum and the maximum deviations of the

Table 2
The surface reaction scheme of the CVD of Al from DMEAA. The kinetic expressions are given by Eq. (4). The units of the pre-exponential factors of each reaction are consistent with Fluent units (Ansys/Fluent 2009).

| ID | Reaction | Pre-exponential factor | Activation energy (kJ $mol^{1}$) |
|---|---|---|---|
| SR1 | $AlH_{3(g)} + 3S \rightarrow AlH_{3(ads)}$ | 4.42 $10^{8}$ m $s^{1a}$ | 19.68[b] |
| SR2 | $AlH_{3(ads)} \rightarrow AlH_{2(ads)} + H_{(ads)}$ | 1.02 $10^{12}$ m $s^{1a}$ | 19.25[c] |
| SR3 | $AlH_{2(ads)} + H_{(ads)} \rightarrow AlH_{3(ads)}$ | 5.11 $10^{12}$ $m^{4}$ $kmol^{1}$ $s^{1a}$ | 18.41[c] |
| SR4 | $AlH_{2(ads)} \rightarrow AlH_{(ads)} + H_{(ads)}$ | 4.98 $10^{12}$ m $s^{1a}$ | 37.43[c] |
| SR5 | $AlH_{(ads)} + H_{(ads)} \rightarrow AlH_{2(ads)}$ | 1.05 $10^{14}$ $m^{4}$ $kmol^{1}$ $s^{1a}$ | 8.37[c] |
| SR6 | $AlH_{(ads)} \rightarrow Al_{(s)} + H_{(ads)}$ | 2.93 $10^{10}$ m $s^{1a}$ | 76.82[c] |
| SR7 | $2H_{(ads)} \rightarrow H_{2(g)} + 2S$ | 5.50 $10^{14}$ $m^{4}$ $kmol^{1}$ $s^{1a}$ | 12.55[c] |
| SR8 | $H_{2(g)} + 2S \rightarrow 2H_{(ads)}$ | 3.07 $10^{10}$ m $s^{1a}$ | 76.97[c] |
| SR9 | $AlH_{3(ads)} \rightarrow AlH_{3(g)} + 3S$ | 2.38 $10^{16}$ m $s^{1a}$ | 86.84[d] |

[a] This work.
[b] Aviziotis et al. (2015) and this work.
[c] Nakajima et al. (2003).
[d] Chaudhuri et al. (2008).

deposition rate and include potential overestimations of the incu-bation time. The simulations performed with the detailed chem-istry pathway proposed in this work correspond to the solid line with triangles. The results obtained by using the simplified chem-istry mechanism (Aviziotis et al., 2015) are also presented (dashed line with stars) for comparison. Observations of the experimental results reveal that it is difficult to distinguish the reaction-limited regime from the diffusion-limited regime, and this has also been reported by Jang et al. (1998). Despite this ambiguous behav-ior, a trend corresponding to a reaction-limited regime can be iden-tified up to 185 LC through the increase of the deposition rate up to this temperature, in good agreement with previous works (Jang et al., 1998; Yun et al., 1998a). There is a potential overestimation of the incubation time for the lowest $T_S$ resulting in the overesti-mation of the growth rate at 130 LC (Aviziotis et al., 2015, 2017) and this accounts for the misfit between the simulated and the experimental results at this $T_S$. At temperature higher than 185 LC, the deposition rate slightly decreases prior to a steep reduction at the highest temperature of the investigated range and the pro-cess is controlled by transport and competitive phenomena which have been considered in the detailed model.

The computational predictions with the detailed chemistry mechanism show satisfactory agreement with the experimental data in the whole temperature range, since they lie within the experimental deviations. In particular, at low temperature the model predicts with sufficient accuracy the measured deposition rate, except the point corresponding at 167 LC, which is off the trend clearly defined from the experimental result. The deposition rate at higher temperature can also be predicted successfully, espe-cially at the highest investigated temperature of 241 LC, which is the major improvement compared to the simplified model. At this temperature, the computational model is capable of predicting the steep decrease of the deposition rate accurately.

We now further explore the successful prediction of the behav-ior of the deposition rate. We compare the G1 gas phase reaction rate (Table 1) at two temperature values, 151 LC corresponding to the reaction-limited regime and 241 LC, where the abrupt decrease of the rate is observed.

Fig. 3 shows the gas phase decomposition rate of DMEAA (reac-tion G1) in the reactor at 151 LC (Fig. 3(a)) and at 241 LC (Fig. 3(b)). At the inlet of the reactor where the temperature is 100 LC, the decomposition of the precursor has already occurred. As the mix-ture moves within the tube the rate slightly decreases, since the temperature in this domain is lower. Before the exit from the shower plate, the values of the gas phase decomposition rate of the precursor for the two temperature values are similar. However, when the mixture approaches the susceptor, the decomposition rate increases as the temperature at this point of the reactor is higher. This increase is more pronounced at $T_S$ = 241 LC (Fig. 3b).

The revealed elevated decomposition rate of DMEAA at 241 LC should lead to a higher concentration of $AlH_3$ between the shower head and the susceptor than at 151 LC. Fig. 4 presents the mass fraction of $AlH_3$ for these two temperature values in the reactor. Contrary to expectations, it can be seen that the concentration of $AlH_3$ is lower at $T_S$ = 241 LC than that at 151 LC. Indeed, at the low-est deposition temperature the mass fraction of $AlH_3$ reaches its maximum value of $4.98\ 10^{3}$ in the area enclosed by the show-erhead and the susceptor. On the other hand, the corresponding value at 241 LC varies between $1.2\ 10^{3}$ and $3.7\ 10^{3}$, when moving from the susceptor to the showerhead, respectively. That is, the available $AlH_3$ at the surface level is four time less at $T_S$ = 241 LC.

Fig. 5 depicts the reaction rate of the $AlH_3$ dimerization (Reac-tion G2 – Table 2). This reaction requires high activation energy in order to occur and it is thus favored at high process temperature. This is confirmed in Fig. 5 which reveals that at 241 LC the reaction

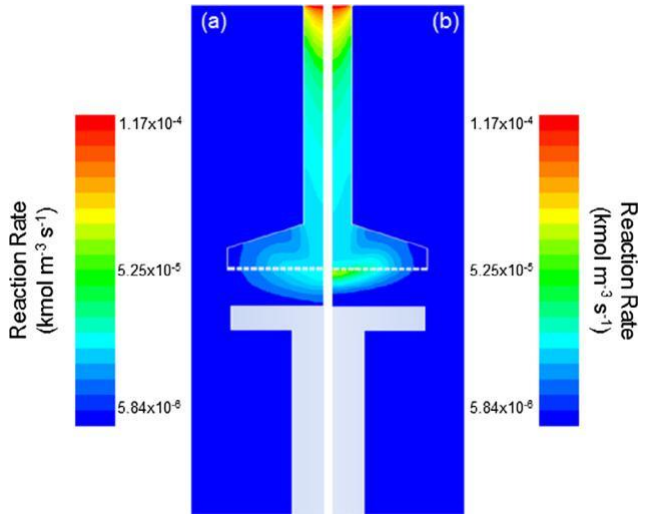


Fig. 3. The gas phase decomposition rate of DMEAA (Reaction G1 – Table 1) at (a) $T_s$ = 151 LC and (b) $T_s$ = 241 LC.

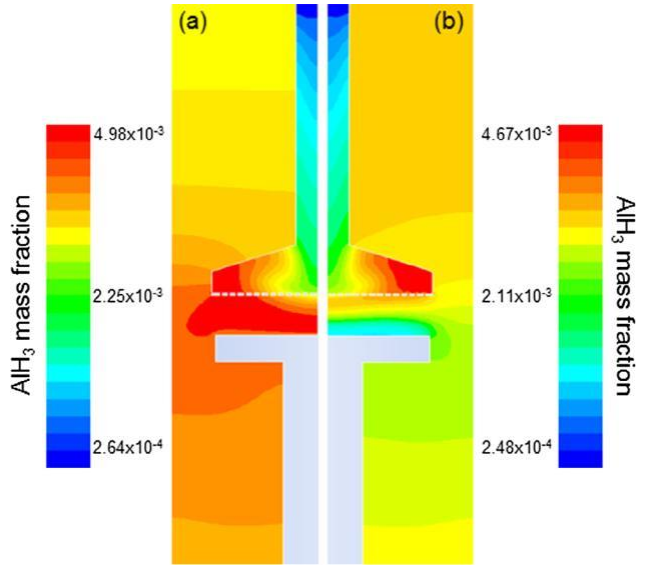


Fig. 4. The distribution of the $AlH_3$ mass fraction in the CVD reactor at (a) $T_s$ = 151 LC and (b) $T_s$ = 241 LC.

rate of G2 is twenty times higher than that at 151 LC. It should be noted that G2 occurs only close to the surface where the tempera-ture is elevated. A direct conclusion of this discussion is that the oligomerization reactions of $AlH_3$, starting from G2, are activated at high temperatures. These reactions result in the depletion of $AlH_3$ in the gas phase. In turn, this impacts the surface processes and the deposition rate, since the consumed $AlH_3$ is not available to be adsorbed on the surface and activate the proposed surface reaction pathway for the deposition of Al.

In addition to the effect of the gas phase reactions on the pro-cess, we also examine the behavior of the surface processes as a function of the surface temperature. Fig. 6 shows in the form of his-togram the rates of the surface reactions at $T_s$ = 151 LC (simple col-umn bars) and $T_s$ = 241 LC (pattern column bars). The two histograms include only reactions that have measurable rates and not reactions which give negligible or zero rates. It is observed that forward reactions have higher rates than the corresponding reverse reactions and consequently, the deposition of Al is feasible.

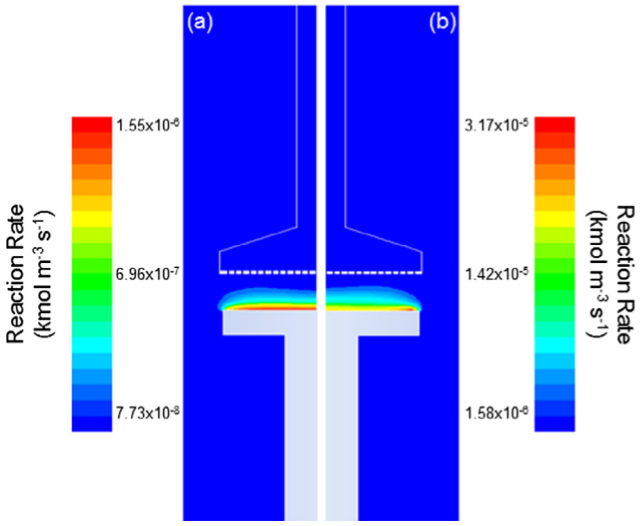


Fig. 5. The gas phase dimerization rate of $AlH_3$ (Reaction 2 – Table 1) at (a) $T_s$ = 151 LC and (b) $T_s$ = 241 LC.

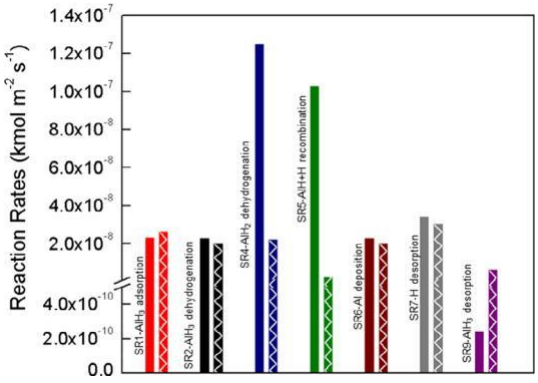


Fig. 6. The surface reactions rates as extracted from the computations with the proposed chemistry scheme at $T_s$ = 151 LC and $T_s$ = 241 LC. Simple column bars correspond to the former $T_s$ whereas patterned column bars to the latter.

At low temperature, the reactions which describe the decomposi-tion of $AlH_2$ to AlH and H and the reverse process (SR4 (blue) and SR5 (green) – Table 2) have significantly higher rates than the rest of the surface reactions. This can be attributed both to the abundance of reactants for these reactions and to their thermo-dynamic advantage due to their kinetic parameters. Furthermore, the rates of $AlH_3$ adsorption (SR1 (red) – Table 2), $AlH_3$ decompo-sition (SR2 (black) – Table 2) and H desorption (SR7 (grey) – Table 2) seem to be similar for both $T_s$, while the re-adsorption of $H_2$ on the surface appears to be negligible.

However, the major finding in Fig. 6 is that the rate of desorp-tion of alane (SR9 (purple) – Table 2) is approximately thirty times higher at the high $T_s$ compared to the corresponding rate at $T_s$ =
151 LC. In particular, the reaction rate at $T_s$ = 241 LC is 6.3 $10^{9}$ kmol $m^{2}$ $s^{1}$, while at $T_s$ = 151 LC is 2.2 $10^{10}$ kmol $m^{2}$ $s^{1}$. It
is this increase of the $AlH_3$ desorption which contributes signifi-cantly to the steep reduction of the Al deposition rate at high tem-perature. That is, at high temperature the increased $AlH_3$ desorption renders it unavailable for the surface processes and eventually, the deposition rate decreases.

We further investigate the surface composition through the amount of each intermediate species. Fig. 7 presents the surface coverage of $AlH_3$, $AlH_2$, AlH and H as well as the unoccupied Al sur-face sites in the form of logarithmic scale histogram at $T_s$ = 151 LC

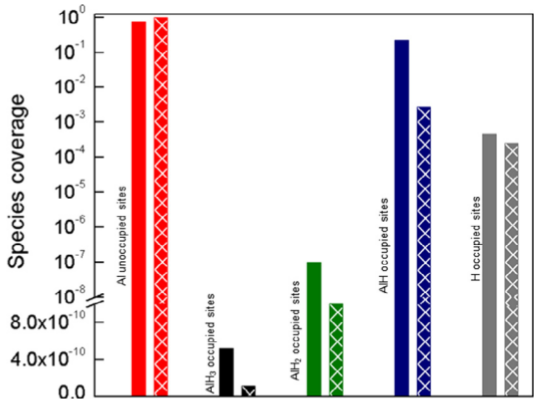


Fig. 7. The surface coverage of Al, $AlH_3$, $AlH_2$, AlH and H at $T_s$ = 151 LC and $T_s$ = 241 LC. Simple column bars correspond to the former $T_s$ whereas patterned column bars to the latter.

(simple column bars) and at $T_s$ = 241 LC (pattern column bars). It can be seen that the surface coverage varies with $T_s$. In particular, at 151 LC the bare Al unoccupied surface sites represent approxi-mately 77.5% of the total surface sites. The rest of the surface sites are occupied mainly by the intermediate AlH ( 22.5%) and by a small amount of atomic H (0.05%). The surface coverage of the remaining species, $AlH_3$ and $AlH_2$, is negligible. On the other hand, at 241 LC the bare Al unoccupied surface sites almost represent the whole surface (99%), and the adsorbed species follow the same order as before (AlH > H > $AlH_3$ > $AlH_2$). The difference in the per-centage of the unoccupied Al surface sites between the two $T_s$ can be explained as before by the elevated desorption rates which have the same order of magnitude as the adsorption rates. The higher amount of AlH at the surface compared to the other inter-mediate species is consistent with literature findings (Nakajima et al., 2003).

## 5. Conclusions

Chemical vapor deposition of aluminum films from dimethylethylamine alane is investigated with the aim to under-stand and control the Al deposition rate at surface temperature in the range 139–241 LC. To meet this objective, we propose a new chemistry pathway for the process based on our combined experimental and computational findings and previous published results.

The Arrhenius plot of the process reveals two regimes; the reaction-limited regime, where the Al deposition rate increases with temperature, prevails within the temperature range 139– 185 LC. At the latter temperature the deposition rate reaches its maximum value and above this temperature starts decreasing. At the highest investigated temperature, the Al deposition rate decreases abruptly due to the increased desorption from the sur-face and the prevailing of gas phase oligomerization reactions. The macroscopic computational model including the proposed chemistry mechanisms of the process (3 gas phase reactions and 9 surface processes) predicts the deposition rate in the examined temperature range with sufficient accuracy, especially at the high-est temperature where previous models have failed.

The model reveals that the decrease of the Al deposition rate at high temperature is attributed to the activation of oligomerization reactions of $AlH_3$ which is depleted in the gas phase. As a result, $AlH_3$ is not available for surface reactions and the deposition rate decreases. Furthermore, by studying the dependence of the surface reactions on the temperature, it is observed that the increased $AlH_3$ desorption rate at high temperature results

in the decrease of the Al deposition rate. Taking into account that the dimerization rate of $AlH_3$ is four orders of magnitude higher than the corresponding desorption rate of $AlH_3$ from the surface, the primary cause of the abrupt decrease of the deposition rate at higher temperature is the activation of $AlH_3$ oligomerization reactions. However, sur-face desorption of $AlH_3$ contributes also to the reduction of the Al deposition rate. Thus, the computational model reveals the two main reasons for the reduction of the deposition rate at high temperature.

## Acknowledgements

I.G.A. acknowledges the financial support provided by the National Scholarship Foundation of Greece (IKY-Siemens Program, Grant number: #SpnD/11160/13b). Partial funding was provided the Institut Français du Petrole et des Energies Nouvelles (IFPEN through the contract #268821, and support by the European Inte-grated Center for the Development of New Metallic Alloys and Compounds (C-MAC) for support. Marius Ozenil, student at the University of Vienna, contributed to this work during his summer 2016 internship at the National Technical University of Athens.

## References

Aitken, C., Harrod, J.F., 1985. Alkyl dichloroacetates: a novel application in the preparation of highly functionalised aziridines from imines. J. Organomet. Chem. 280, C11–C13.

Aloui, L., Duguet, T., Haidara, F., Record, M.-C., Samélor, D., Senocq, F., Mangelinck, D., Vahlas, C., 2012. Al-Cu intermetallic coatings processed by sequential metalorganic chemical vapor deposition and post deposition annealing. Appl. Surf. Sci. 258, 73–80.

Amazawa, T., Yamamoto, T., Arita, Y., 1998. Planarized multilevel interconnection using chemical mechanical polishing of selective CVD–Al via plugs. IEEE Trans. Electron Dev. 45, 815–820.

Ansys/Fluent v12.1sp1. Documentation. Ansys Inc., 2009.

Armbrüster, M., Konvir, K., Friedrich, M., Teschner, D., Wowsnick, G., Hahne, M., Gille, P., Szentmiklósi, L., Feuerbacher, M., Heggen, M., et al., 2012. $Al_{13}Fe_4$ as a low-cost alternative for palladium in heterogeneous hydrogenation. Nat. Mater. 11, 690–693.

Aviziotis, I.G., 2016. Chemical Vapor Deposition of Al, Fe and of the Al13Fe4 Approximant Intermetallic Phase: Experiments and Multiscale Simulations. Ph. D. Thesis, National Technical University of Athens, Greece.

Aviziotis, I.G., Duguet, T., Soussi, K., Kokkoris, G., Cheimarios, N., Vahlas, C., Boudouvis, A.G., 2015. Investigation of the kinetics of the chemical vapor deposition of aluminum from dimethylethylamine alane: experiments and computations. Phys. Status Solidi C 12, 923–930.

Aviziotis, I.G., Cheimarios, N., Duguet, T., Vahlas, C., Boudouvis, A.G., 2016. Multiscale modeling and experimental analysis of chemical vapor deposited aluminum films: linking reactor operating conditions with roughness evolution. Chem. Eng. Sci. 155, 449–458.

Aviziotis, I.G., Duguet, T., Vahlas, C., Boudouvis, A.G., 2017. Combined macro-/nano-scale investigation of the CVD of Fe from $Fe(CO)_5$. Adv. Mater. Interf. 1601185, 1–10.

Chaudhuri, S., Rangan, S., Veyan, J.-F., Muckerman, J.T., Chabal, Y.J., 2008. Formation and bonding of alane clusters on Al(111) surfaces studied by infrared absorption spectroscopy and theoretical modeling. J. Am. Chem. Soc. 130, 10576–10587.

Cheimarios, N., Kokkoris, G., Boudouvis, A.G., 2010. Multiscale modeling in chemical vapor deposition processes: coupling reactor scale with feature scale computations. Chem. Eng. Sci. 65, 5018–5028.

Choy, K.L., 2003. Chemical vapour deposition of coatings. Prog. Mater. Sci. 48, 57– 170.

Deen, W.M., 1998. Analysis of transport phenomena. Oxford University Press, New York, USA.

Delmas, M., Poquillon, D., Kihn, Y., Vahlas, C., 2005. Al-Pt MOCVD coatings for the protection of Ti6242 alloy against oxidation at elevated temperature. Surf. Coat. Technol. 200, 1413–1417.

Frigo, D.M., van Eijden, G.J.M., Reuvers, P.J., Smit, C.J., 1994. Preparation and properties of alane dimethylethylamine, a liquid precursor for MOCVD. Chem. Mater. 6, 190–195.

Hamasha, M.H., Alzoubi, K., Switzer III, J.C., Lu, S., Desu, S.B., Poliks, M., 2011. A study on crack propagation and electrical resistance change of sputtered aluminium thin film on poly ethylene terephthalate substrate under stretching. Thin Solid Films 519, 7918–7924.

Han, J.S., Jensen, K.F., Senzaki, Y., Gladfelter, W.L., 1994. Pyrolytic laser assisted chemical vapor deposition of Al from dimethylethylamine-alane: Characterization and a new two-step writing process. Appl. Phys. Lett. 64, 425–427.

Hersee, S.D., Ballingal, J.M., 1990. The operation of metalorganic bubblers at reduced pressure. J. Vac. Sci. Technol. A 8, 800–804.

Jang, T.W., Moon, W., Baek, J.T., Ahn, B.T., 1998. Effect of temperature and substrate on the growth behaviors of chemical vapor deposited Al films with dimethylethylamine alane source. Thin Solid Films 333, 137–141.

Kawamura, H., Kumar, V., Sun, Q., Kawazoe, Y., 2003. Cyclic and linear polymeric structures of $Al_nH_{3n}$ (n=3-7) molecules. Phys. Rev. A 67 (063205), 1–8.

Kim, B.-Y., Li, X., Rhee, S.-W., 1996. Microstructure and deposition rate of aluminum thin films from chemical vapor deposition with dimethylethylamine alane. Appl. Phys. Lett. 68, 3567–3569.

Kleijn, C.R., 2000. Computational modeling of transport phenomena and detailed chemistry in chemical vapor deposition – a benchmark solution. Thin Solid Films 365, 294–306.

Kleijn, C.R., Dorsman, R., Kuijlaars, K.J., Okkerse, M., van Santen, H., 2007. Multi-scale modeling of chemical vapor deposition processes for thin film technology. J. Cryst. Growth 303, 362–380.

Kuwana, K., Li, T., Saito, K., 2006. Gas-phase reactions during CVD synthesis of carbon nanotubes: Insights via numerical experiments. Chem. Eng. Sci. 61, 6718–6726.

Lee, H.M., Seo, J.Y., Jung, A., Choi, S.-Y., Ko, S.H., Jo, J., Park, S.B., Park, D., 2014. Longterm sustainable aluminum precursor solution for highly conductive thin films on rigid and flexible substrates. ACS Appl. Mater. Interf. 6, 15480–15487.

Letterman, R.D., Iyer, D.R., 1985. Modeling the effects of hydrolyzed aluminum and solution chemistry on flocculation kinetics. Environ. Sci. Technol. 19, 673–681.

Luo, B., Gladfelter, W.L., 2009. Chemical vapor deposition of metals: W, Al, Cu and Ru. In: Jones, A.C., Hitchman, M.L. (Eds.), Chemical Vapor Deposition: Precursors, Processes and Applications. Elsevier Ltd., Oxford, p. 329.

Masu, K., Yokoyama, M., Matsuhashi, H., Tsubouchi, K., 1994. Contribution of free electrons to Al CVD on a Si surface by photo-excitation. Appl. Surf. Sci. 79–80, 237–243.

Matsuhashi, H., Lee, C.-H., Nishimura, T., Masu, K., Tsubouchi, K., 1999. Superiority of DMAH to DMEAA for al CVD technology. Mater. Sci. Semicond. Process. 2, 303–308.

Michos, F.I., Sgouros, A.P., Sigalas, M.M., 2016. Ab initio study of boron and aluminum hydrides nanoparticles. Int. J. Hydrogen Energy 41, 20210–20216.

Nakajima, T., Nakatomi, M., Yamashita, K., 2003. Quantum chemical calculations on Al-CVD using DMEAA: surface reaction mechanism of $AlH_3$ on Al(111). Mol. Phys. 101, 267–276.

Robinson, D.W., Rogers Jr, J.W., 2000. Low temperature atomic layer growth of aluminum nitride on Si(100) using dimethylethylamine alane and 1,1-dimethylhydrazine. Thin Solid Films 372, 10.

Simmonds, M.G., Taupin, I., Gladfelter, W.L., 1994. Selective area chemical vapor deposition of aluminum using dimethylethylamine alane. Chem. Mater. 6, 935– 942.

Sundman, B., Ohnuma, I., Dupin, N., Kattner, U.R., Fries, S.G., 2009. An assessment of the entire Al–Fe system including $D0_3$ ordering. Acta Mater. 57, 2896–2908.

Tan, C.M., Roy, A., 2007. Electromigration in ULSI interconnects. Mater. Sci. Eng. R Rep. 58, 1–75.

Vahlas, C., 2010. Chemical vapor deposition of metals: from unary systems to omplex metallic alloys. In: Belin-Ferré, E. (Ed.), Surface Properties and Engineering of Complex Intermetallics, Book Series on Complex Metallic Alloys, vol. 3. World Scientific, Singapore, pp. 49–81.

Xenidou, T.C., Boudouvis, A.G., Markatos, N.C., Samélor, D., Senocq, F., Prud'homme, N., Vahlas, C., 2007. An experimental and computational analysis of a MOCVD process for the growth of Al films using DMEAA. Surf. Coat. Technol. 201, 8868– 8872.

Xenidou, T.C., Prudhomme, N., Vahlas, C., Markatos, N.C., Boudouvis, A.G., 2010. Reaction and transport interplay in Al MOCVD investigated through experiments and computational fluid dynamic analysis. J. Electrochem. Soc. 157, D633–D641.

Yun, J.-H., Kim, B.-Y., Rhee, S.-W., 1998a. Metal-organic chemical vapor deposition of aluminum from dimethylethylamine alane. Thin Solid Films 312, 259–264.

Yun, J.-H., Park, M.-Y., Rhee, S.-W., 1998b. Fourier transform infrared diagnostics of gas phase reactions in the metalorganic chemical vapor deposition of aluminum from dimethylethylamine alane. J. Vac. Sci. Technol. A 16, 419–423.